# Narrowband spectroscopy on subwavelength hole arrays in thin gold films using high-speed spectrum scanning

Adriaan van der Feltz

under supervision of dr. D. van Oosten
at the Debye Institue

June 19, 2013

**Abstract**

Generally spectroscopy is conducted using a broadband incident light spectrum. In this study we present and evaluate a novel technique using an acousto-optic tuneable filter to filter out narrowband spectra and conduct spectroscopy measurements using these narrowbanded spectra one at a time. By scanning through the entire spectrum at high speed a full spectroscopy spectrum can be measured. This method provides a solution to increase the intensity relative to the entire spectrum of otherwise weakly present wavelengths, resulting in a better noise to signal ratio. The transmission spectroscopy is conducted on sub-wavelength hole arrays in a thin gold film. Exotic optical phenomena like extraordinary optical transmission are expected for these type of samples. However the results do not show the expected anomalies in the transmission graph. Comparing our results with transmission measurements from earlier conducted research on the same samples using a more established spectroscopy method shows a deviating outcome. Positive results are found for the measured values at the borders of the spectrum, where due to the increased relative intensity the measurements show a much clearer graph.

# Contents

# 1 Introduction

The aim of this research is to develop a new experimental setup based on a novel method in spectroscopy using a high-speed scan through the near-visible wavelength spectrum. Using this method we investigate the transmission through nanoscale hole arrays in thin gold films and evaluate the results with established spectroscopy techniques. The advantage of this method is in the filtering of the spectrum before the illumination of the sample enabling spectroscopy measuring on selective wavelengths in contrast to illumination the sample with a broad spectrum with high total intensity. By gauging this possibility in spectroscopy we propose an accurate solution for fast high intensity-per-wavelength measurements without overexposing the sample. We are especially interested in transmission spectrometry for different arrays using a spectrum in the $500nm - 1000nm$ range.

The analysis of the transmission on these pre-fabricated arrays is furthermore a preliminary study, by which in the long run we hope to achieve better understanding on light-matter interaction on nanoscale hole arrays fabricated with femtosecond laser ablation. Following the research done by *Hao Zhang et al.* on femtosecond single shot laser ablation[15], it is our goal to revise that experimental setup into a more rigid fashion for future research on these arrays by implementing this new spectroscopy method.

# 2 Theory

In this chapter the relevant theory describing light-matter interactions are set forth. Contemporary research is being conducted into the possibilities of using light in the form of high-intensity ultra-short laser pulses to ablate material[2][3] for micro-lithography purposes[8]. Using these pulses to ablate hole arrays in materials affects the transmission of incident laser beams. By varying the array properties the transmission is influenced. With this technique the way the material interacts with optical signal can be altered, which for instance has potential applications in optoelectronic devices.

This transmission can be studied using spectroscopy for which a basic description covering the theory and the pros and cons of established spectroscopy techniques is given. In order to study the transmission of these particular arrays a novel technique is introduced to filter wavelengths out broad laser spectra using an acousto-optic tuneable filter. Furthermore a solely classic physical approach proves to be insufficient in explaining the transmission spectrum and modern concepts like extraordinary optical transmission are introduced to provide a satisfactory description.

## 2.1 Optical Transmission Spectroscopy

Spectroscopy is an empirical technique based on the interaction between light and matter to study either of them. Ordinarily in the case of transmission spectroscopy broadband optical plane waves illuminate a sample through which the light is transmitted (e.g. due to translucence or holes) and afterwards the transmission is measured. Comparison of the transmitted spectrum with the incident spectrum reveals the influence of the sample on specific wavelengths.

### 2.1.1 Classical Optical Transmission

Theory offers us useful insight as what to is expected of the transmission on nanoscale array. Classically the total power of light with a certain intensity transmitted through large holes ($r > \lambda$) is easily found to be:

$$P = A_{\perp} I \tag{2.1}$$

with $I$ being the incident intensity and $A_{\perp}$ the effective hole area depending on the angle of incidence. Intuitively one can see that for holes with a diameter far greater than the transmitted wavelength most of the light gets transmitted without interaction with the material due to the distance as can be seen in figure (2.1a).

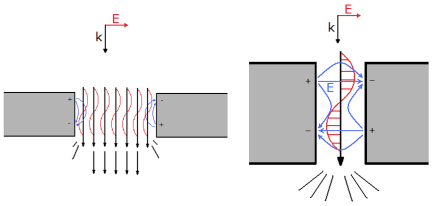


(a) Light transmitted through an aperture of $r > \lambda$

(b) Light transmitted through an aperture of $r \ll \lambda$

Figure 2.1: Schematic overview of light travelling through different size apertures. Figures from [10]

However for holes with ($r \ll \lambda$) a relative large portion of the light is very close to the material or maybe even reflects onto it. In the case of conductors like metals the light induces an electric field causing a charge distribution and accordingly the electrons will interact with the light as depicted in figure (2.1b), affecting the transmission. Since the ratio between the hole area and the incident wavelength clearly are of importance, equation (2.1) needs to be adjusted for the transmitted power[1, p. 173]. Bethe also gives a description for the field[1, p. 169] of the diffracted light. In equation (2.2) $k$ is the wavevector of the incident wave and $r$ the hole radius while $P$ and $I$ are unchanged. For (2.2) $x$ is the distance from the diffraction plane:

$$P = I\,\frac{64\pi}{27}k^4 r^6 \tag{2.2}$$

$$\psi_0\,(x) = \frac{e^{ikx}}{x} \tag{2.3}$$

For a transmission sample with multiple periodic apertures interference also needs to be taken into account. According to Huygens' Principle[11, p. 1235] the transmission on a sub-wavelength hole array can be thought of as $N$ individual radiating sources, that can interfere con or destructively leading to a interference pattern, according to:

$$\lambda = \frac{d\sin\theta}{m} \tag{2.4}$$

for which $d$ is the periodicity between consecutive sample holes, $\theta$ the angle of diffraction due to the sample and $m$ the order of inference maximum. Since the

transmitted total energy needs to be conserved the transmitted beam intensity is spread out over the diffracted maxims. Equation (2.4) shows that such a maximum in the transmitted intensity can be expected in the measured spectrum whenever the incident wavelength $\lambda$ is a integer multiple of the sample specific ratio of $^{d}/_{n}$ known as the Rayleigh anomaly.

Bethe's equations give a rough idea of aperture transmission and the wavelength dependent diffraction, however they do not provide insight in the physics involved in the wavelength dependent interaction of the light with the aperture causing it. Moreover contemporary research shows that the diffracted light does not at all diffracts isotropically[1] as would be expected from Bethe. For certain wavelengths much stronger transmission is measured near to the sample surface. This 'extraordinary optical transmission' (EOT) phenomenon can not be explained exclusively by the above mentioned theories, indicating additional effects.

### 2.1.2 Extraordinary Optical Transmission

Incident light interacting with solid metal materials effectively is the interacting of optical photons with the induced electrons, which form a collective electron plasma with quantized excitations called surface plasmons (SP)[6, p. 390]. Light-plasmon coupling as a surface plasmon polariton (SPP) is one the main causes for EOT along others[2] and extensive research has been conducted on the subject the last decade. An exhaustive treating of these phenomena goes beyond this particular research, there are many publications on EOT for a more elaborate treatise[4, 9, 14, 12, 13], however a brief overview will be presented here. The main focus here is to gain a quantitative frame of reference from theory to know what results we can expect from the measurements. The most important aspects of a SPP model for EOT are: the induction of an electric field in the metal surface, the forming of an electron plasma, the behavior of the plasmons, the coupling of light to the plasmons states into a surface plasmon polariton.

**Optical induced E-fields and near surface electron plasma**
In the following paragraphs the metal sample considered is a smooth surface without any apertures. These metals, like gold, are good conductors because of their high electron density $n_e \sim 10^{28} m^{-3}$ and automatically high charge density $q_e = e\, n_e$. When an electromagnetic-wave strikes the surface it penetrates the material up to a specific skin-depth $\delta = \sqrt{\frac{2}{\omega \mu_0 \sigma}}$[6, p. 396] with $\omega$ the optical frequency, $\mu_0$the magnetic susceptibility and $\sigma$ the materials conductivity. A

[1] Invariant with respect to direction

[2] SPP is largely dependent on the resonance (2.12) with incident light and should not have a great contribution for non-visible wavelength spectra. Evanescent wave coupling is suggested[5] as another possible explanation

decaying electric field is induced for that depth in the material which results in a force on the electron distribution. Simplifying that this involves a constant field, it initially only forces the electrons a distance $u$ out of their equilibrium. The result is a net-force $F(u) = \frac{-e\,q_e}{\epsilon_0}u$ trying to restore the initial condition. The whole process can be visualized a a harmonic oscillator with $F(r) = m_e\frac{d^2r}{dt^2}$:

$$r(t) = r_0 e^{i\omega_p t} \tag{2.5}$$

$$\text{with } r_0 = u \text{and } \omega_{SP} = \sqrt{\frac{e\,q_e}{2\,m_e\epsilon_0}} \tag{2.6}$$

In the above equations $e$ and $m_e$are the electron charge and mass, $\omega_{SP}$ is the oscillation frequency of the collective electron liquid or plasma, for near surface plasma a factor 2 is added because the metal surface extends only half into the total space. The oscillation energies are quantized in quanta of $\hbar\omega_{SP}$. These quanta are often described as quasi-particles called surface plasmons (SP).

**Surface Plasmons and Surface Plasmon Polaritons**

Whenever surface plasmons are present at the metal surface incident photons can couple to its oscillation and form a surface plasmon polariton (SPP). Polaritons are quasi-particles constituted of a photon strongly coupled to a electric or magnetic excitation, in this case the SP. That way the light is not immediately transmitted or reflected but more or less confined along the surface of the metal in a oscillating state as illustrated in figure (2.2), the SPP. Solving the Maxwell equations[3][10] shows how these SPP's travel along the surface and into the material with a certain wavelength ($\lambda_{SPP} \sim k_{SPP}^{-1}$):

$$k_{SPP}^{\parallel} = k_0\sqrt{\frac{\epsilon_d\epsilon_m}{\epsilon_d+\epsilon_m}} \tag{2.7}$$

$$k_{SPP}^{\perp} = k_0\sqrt{\frac{\epsilon_m^2}{\epsilon_d+\epsilon_m}} \tag{2.8}$$

In (2.7) and (2.8) $k_0$ is the vector in vacuum and $\varepsilon_d$ and $\epsilon_m$ are the electric permittivity of a dielectricum (e.g. air) and the metal. Note that equations (2.7) and (2.8) also show that the absolute value $k_{SPP}$ is directly related to the wavelength of the coupled light.

Also since $\epsilon_m$ is always complex for metals, the traveling SPP decays and the length of this decay-depth can be calculated in the metal's z-direction:

[3]Deducing this behavior surpasses the aim of this study. This is however treated in other publications

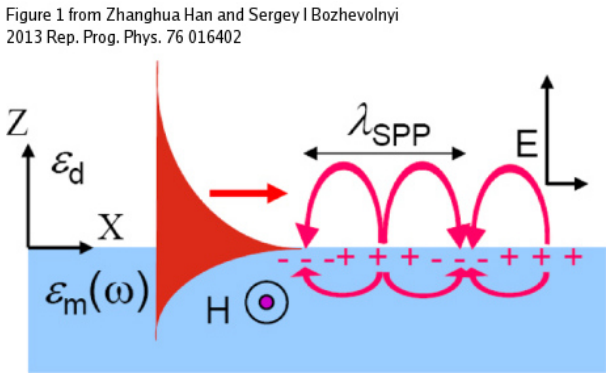


Figure 2.2: Schematic display of a metal-dielectric interface with SPP's traveling along the surface with wavelength $\lambda_{SPP}$

$$\delta_{E,m} \approx \frac{\lambda_0}{4\pi\sqrt{\mid \epsilon_m \mid}} \tag{2.9}$$

This distance is a very important parameter in the SPP model for EOT. Given a solid sample with thickness $d < \delta_{E,m}$ it is possible for an impinging photon to couple to a SP on the surface of incidence into a SPP, then travel through the thin film to the other side and at that surface scatter into a SP and a photon.

### 2.1.3 EOT and Multi-hole Diffraction Interference

In section (2.1.2) a brief treating of EOT for smooth samples has been set forth. However in the sample used in the experiments the thin gold film is perforated in a periodic manner resulting in an array of sub-wavelength holes. As we have seen in section (2.1.1) the light n gets diffracted by these apertures but now also EOT needs to be taken into account. Equations (2.7) and (2.8) quantify the k-vectors of the SPP's traveling over the sample surface with according wavelengths. The diffraction on these arrays is a bit more complicated then described by Brags Law[4] (equation (2.4)). The Laue equations describe the diffraction of a k-vector on a reciprocal lattice and for a two dimensional reciprocal lattice array are given by equation (2.11)[6] and solved for (2.11):

$$\begin{aligned} \overrightarrow{k} \cdot \hat{u}_1 &= 2\pi\, p \\ \overrightarrow{k} \cdot \hat{u}_2 &= 2\pi\, q \end{aligned} \tag{2.10}$$

$$k_{laue} = \pm p\frac{2\pi}{P}\hat{u_1} \pm q\frac{2\pi}{P}\hat{u_2} \tag{2.11}$$

[4]Brags Law follows from the Laue equations for a more simple geometric case

In (2.11) $p$ and $q$ are integers and $P$ is the periodicity of the array and $\hat{u}_{1,2}$ are the reciprocal vectors. The diffraction on this array may interfere constructively with the EOT if the k-vector following from equation (2.11) matches that of equation (2.7)$k_{SPP}^{\parallel} = k_{laue}$ and since $k_{SPP}$ is related to the incident wavelength (section (2.1.2)) we can solve for:

$$\lambda_0 = P\sqrt{\frac{1}{p^2+q^2}\frac{\epsilon_m\epsilon_d}{\epsilon_m+\epsilon_d}} \tag{2.12}$$

$\lambda_0$ being the incident wavelength for which we might expect constructive interference.

### 2.1.4 EOT Theory Summary

Section (2.1.2) showed that the incident laser light can couple to the quantified oscillation modes of the electron plasma known as surface plasmons(2.6). The resulting surface plasmon polaritons travel with a certain wavelength (2.7) across the surface and into the bulk of the material for a certain depth (2.9), which can lead to transmission by scattering into light at the opposite surface. For samples with hole arrays a resonance effect might occur when the incident wavelength matches the pitch-dependent ideal diffraction wavelength (2.12).

## 2.2 Spectroscopic Techniques

### 2.2.1 Intensity and spectral resolution

Conventional spectroscopy uses a broadband spectrum to illuminate the sample that is to be studied. However this has its disadvantages. Most importantly no laser has a perfect spectrum in which all wavelengths have equal intensity. Instead the total intensity of the laser will be divided over the various wavelengths disproportionally leading to very high intensity wavelengths and very weak intensities, so weak that they become hard to measure. This lack of intensity will impair for instance a photodiode to accurately detect the transmission at the accompanying wavelengths. The resolving power of a spectrograph is given by

$$R = \frac{\lambda}{\Delta\lambda} \tag{2.13}$$

In which $\Delta\lambda$ is the accuracy with which the spectrograph can distinguish various wavelengths at a wavelength $\lambda$. More intensity per singular wavelength improves the resolving power of the spectrograph resulting in spectrum measurements with better spectral resolution. Simply increasing the output of the laser would not solve this problem. The differences between various wavelengths would

remain and calibration of the photodiode's sensitivity would be necessary to avoid saturation effects. Furthermore other effects could take place like even further ablating the sample due to the high intensity of the total incident laser spectrum. It would be ideal to select narrowband wavelength spectra and be able to do spectroscopy with relative high intensity per wavelength.

### 2.2.2 Acousto-Optic Tuneable Filter

It is known that white light constitutes of multiple wavelengths which is quite commonly observed as rainbows or due to prisms. Both examples diffract the various wavelength due to the wavelength dependency of the refractive index and that way the light is geometrically spread out per wavelength. Other means to filter wavelengths in a continuous spectrum exist with gratings, notch filters or dichroic filters, however each of these have restricted focus ability or lack in wavelength adaptability.

Acousto-optic tuneable filters (AOTF) should offer a solution to select narrowband spectra that also retain the beam profile and its pulse shape. AOTFs apply the acousto-optic effect which describes the diffraction of optical waves due to acoustical ones. The acousto-optic effect is a consequence of the photo-elasticity of a material. A propagating acoustic wave in material causes density fluctuations, just as it does in air. These periodic perturbations cause the optical waves traveling through the AOTF to diffract accordingly as shown in figure(2.3). The acousto-optic effect can be explained by the mechanical strain $\alpha$ in the material due to the acoustics, which causes a change in the permittivity $\epsilon$ and as a result in its diffractive index $n$. A less intuitive but easier break down is by explaining the interaction of the optical photons and the acoustic phonons[7].

$$|k_o| = \frac{\omega n}{c} \tag{2.14}$$

$$|k_a| = \frac{2\pi f}{v_a} \tag{2.15}$$

Both the photons and phonons can be described by the k-vectors in vectorspace. The subscripts $o$ and $a$ in (2.14) and (2.15) respectively denote optical or acoustic signals, $\omega$ is the light frequency, $n$ the material's refractive index, $c$ the speed of light, $f$ the acoustic frequency and $v_a$ the speed of the acoustic signal. The photons and phonons interact according to the k-matching criterion, which dictates:

$$k_o^i \pm k_a = k_o^d \tag{2.16}$$

The superscripts $i$ and $d$ in (2.16) refer to the incident and diffracted optical signals. Equation (2.16) quantifies the influence of the traveling acoustic wave on the transmitted optical signal and this is further illustrated in figure (2.3).

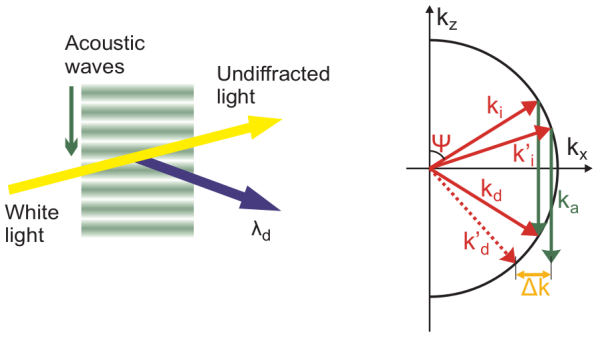


Figure 2.3: **a)** Part of the light travelling through the AOTF gets diffracted by an acoustic traveling wave
**b)** Conceptual illustration of k-matching. The semicircle depicts the dispersion surface for a certain k vector $k_i$. The incident vector gets matched to another point on the dispersion surface according to the acoustic vector $k_a$. For other angles it leads to a k-mismatch
Image from [7]

Considering incident plane optical waves under fixed angle $\Psi$ with a certain $\omega$, it shows that the k-vector has a fixed length $\frac{\omega n}{c}$. As a result the $k_o^i$ vector points onto a hemisphere with equal radius $\frac{\omega n}{c}$. spanned in vector-space, known as the dispersion surface, here depicted in 2D as semicircle. Because of the $\pm$ condition each $k_o^i$ must have a single point on the dispersion surface for which another point $k_o^d$ is matched, given a specific $k_a$. Automatically for the same $k_a$ but an optical signal with a different $k_o^{'i}$, with another angle of incidence k-matching $(k_o^{'i} \pm k_a)$ will lead to a mismatch for which $k_o^{'d}$ does not exist on the dispersion surface and therefore is unphysical.

The AOTF crystal is birefringent, which means that the polarization of the light makes a difference for the speed of the light in the material and its refractive index. The anisotropic[5] crystalline structure of a birefringent material explains this polarization dependence along certain axes along the material. In the case of a single anisotropic axis it is called an uni-axial material. The polarizations are then referenced to this axis as ordinary in the parallel case and extraordinary in the other. Because of the refractive index difference (2.17) due to anisotropy the dispersion surface for either polarization is also stretched out in one direction, which is illustrated in figure (2.4). Now the acoustic k-vector couples each singular ordinary optical k-vector uniquely to a diffracted extraordinary k-vector.

$$\Delta n = n_e - n_o \tag{2.17}$$

The birefringency makes it so that each optical k-vector has a single acoustic

[5] Directional dependent

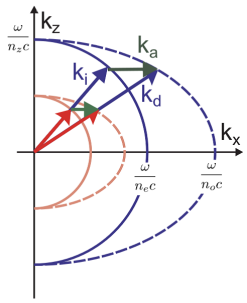


Figure 2.4

matched k-vector. Before, with equation (2.3), there was no selection possible based on exclusive matching. The conclusion is that theoretically for a fixed incident angle $\Psi$ of the broadband spectrum, each separate wavelength is uniquely matched to a specific acoustic frequency and is only diffracted at that acoustic frequency.

The acoustic frequency dependence of the diffracted wavelengths can also be expressed mathematically by

$$\lambda_0 = \frac{v_a}{f_a} \Delta n \, F(\Psi) \tag{2.18}$$

Since the diffracted light is not exactly a single wavelength, $\lambda_0$ refers to the narrowband's central wavelength, $F(\Psi)$ is a function of the angle of incidence, $v_a$, $f_a$ and $\Delta n$ still denote respectively the acoustic wave speed, frequency and the difference in refractive index due to the anisotropy. The bandpass is

$$\Delta\lambda = \frac{0.9\lambda_0^2}{\Delta n \, L \sin^2 \Psi} \tag{2.19}$$

$L$ is the acoustic interaction length and all other variables remain unchanged. The width of the intensity peak of the diffracted transmission of the AOTF can be approximated by the following equation

$$I_T(\lambda) \propto \frac{\sin^2 \lambda}{\lambda} \tag{2.20}$$

A problem for the optimal intensity is illustrated here as due to higher order diffraction multiple other intensity peaks will appear at other wavelengths. This behavior can clearly be seen due to the sine function in equation (2.20). Calibration is needed to confirm the quantitative relation between the acoustic and optical signal as well as the optimal intensity for maximal resolution, which will be addressed in section (3.3).

# 3 Method

In this chapter an overview of the experimental setup and its development is presented as well as the investigated samples and our methodology. The setup used in earlier studies on single-shot ablation femtosecond laser ablation needed to be improved in order to create periodic ablated hole arrays and its examination. Improvement was required in the accuracy of the sample alignment and the flexibility of the setup to easily measure optical sample properties. In this case a solution for high-speed low-intensity spectroscopy is found. A major part of this research was modeling the setup and expanding the setup to fit our new needs. An image of this model is placed in the appendix.

## 3.1 Setup

A main challenge in order to fabricate and examine ablated arrays is to develop the setup used by *Hao Zhang, D. et al.*so that its precision and repeatability during the ablation is sufficient to create nanometer scale periodic hole arrays. Moreover it needs to be adaptable for further measurements on the arrays transmission and possibly future measurements on its reflection etcetera. To this end, the ability needs to be implemented to incorporate multiple wavelengths into the setup for spectroscopy purposes without such high intensity that would over-illuminate the sample.

### 3.1.1 Setup Development

Raised above the original main optical table two new breadboards are added spaced also above each other so that it becomes possible for the beam path to vertically approach the sample.

Precision and repeatability are then achieved by mounting the sample horizontally on a piëzo-stage (Physik Intrumente M-686 XY) on the middle breadboard ensuring sample-stability in the vertical direction and $0,1\mu m$ accuracy while moving the sample in the horizontal plane. The stage-controller is controlled through Python scripts[6] which synchronize the movements with the repetition-rate of the Hurricane, enabling the stage to follow a snake-like path with enough consistency to create arrays of arbitrary size and periodicity.

Centered above the stage a vertical component of the setup is constructed through the top breadboard, composed of an optical tube system attached to a microscope turret enabling the substitution of different microscope objectives for either strong focusing in the case of laser ablation or weakly focused for transmission spectroscopy measurements.

[6] See Appendices

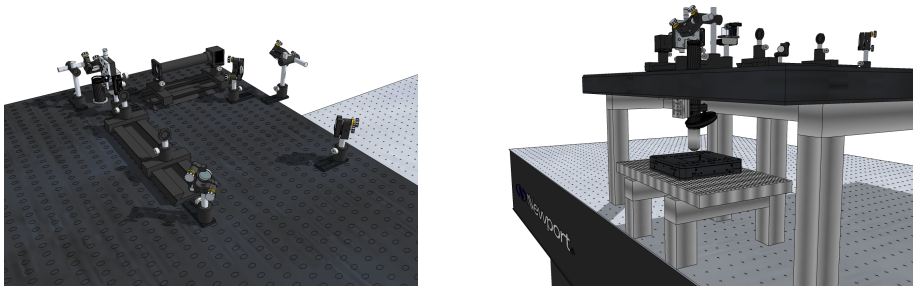

Figure 3.1: Model of the setup used for spectroscopy

On the top board a beamsplitter is placed deflecting the incoming beam in one direction for analysis and deflecting the beam returned by the sample in the other direction to image the sample with the camera for alignment. In the middle breadboard a collimating lens is mounted to collect the transmission which is subsequently focused on a photodiode for measurement.

Adjustable wavelengths are accomplished through the combination of a continuous white light laser with an AOTF enabling to adjust the wavelength of the transmitted beam by varying the frequency of the traveling RF wave through the AOTF. Fast adjustability of the AOTF frequency makes it possible to sweep through the spectrum in milliseconds. The transmitted beam is brought in to the beam path of the main setup completing the development of the new experiment setup.

## 3.2 Laser

### 3.2.1 Beam-profiling and spectrum

The incorporation of the AOTF meant a spectrum of wavelengths that needed to be focused on the sample structure in a setup that formerly contained only a singular wavelength. Most optical component should be achromatic with exception of the beamsplitter. Using a beamprofiling camera the beam profile was measured at the sample surface for various wavelengths. It is important to be able to position and focus the spot so that it is confined within the array area.

The beam profile was analyzed using DataRay Inc. software. Clipping the beam profile at $13,5\%$ the spot diameter was determined to stay within $30\mu m$ with an optimum of $23,7\mu m$ at a wavelength of $720nm$. This confirms the ability to focus the spot enough to be confined within the array area.

### 3.2.2 Laser spectrum

The laser used for the experiments is a NKT Photonics SuperK Extreme EXR-4(A). The laser spectrm was measure using a spectrometer (Ocean Optics HR2000CG-UV-NIR). Figure (3.2) shows the spectrum, which was in good agreement with spectrum described in technical propertie describtion. It accounts for the sudden increases in transmission measured in section (4.1.1).

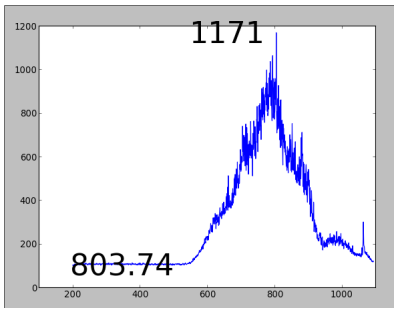


Figure 3.2: NKT Photonics SuperK Extreme EXR-4 as measured with spectrometer

## 3.3 AOTF Calibration

The acoustic frequency was changed rapidly in time scanning through the entire region. The AOTF needed to be calibrated to find the following diffracted wavelength as a function of time. This was done by measuring the spectrum with a spectrometer (Ocean Optics HR2000CG-UV-NIR) for small step changes ($0.4\,MHz$) in the acoustic frequency. According with the speed with which the acoustic frequency was increased, was the resulting wavelength determined. The relation is illustrated in figure (3.3).

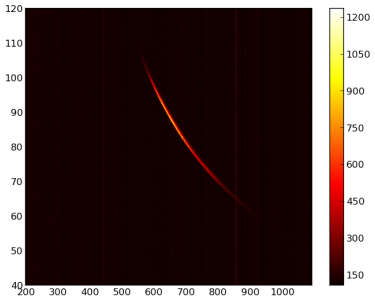


Figure 3.3: Relation between the inputted acoustic frequency and the resulting wavelength. The y-axis is the acoustic frequency in $MHz$ and the x-axis represents the diffracted ligth's wavelength in $nm$

## 3.4 Sample

The studied sample was a collection constituted out of 82 nanoscale hole arrays in a thin gold film on glass created using an electron beam lithography and lift-off. Figures (3.4a) and (3.4c) are made using SEM imagaing, giving an overview of the entire sample. Over the entire roster the E-beams lithographic parameters are varied per array, resulting in various arrays. It are the individual arrays we are interested in. The aimed hole diameter is changed in the vertical direction and the E-beam exposure time is altered in the horizontal direction. The resulting holes depend on the ratio between these two parameters, leading in some cases to underdeveloped holes. Therefore some arrays are unsuitable for transmission spectroscopy due to defects in the periodicity of the array. Finally the pitch between consecutive holes within an array also differs per array.

Taking in account these requirements we selected 9 arrays of acceptable quality indicated by the indices $\alpha$ through $\rho$. Notably all of them lay more or less on the diagonal indicating an optimal ratio in E-beaming parameters. Each square array has an $50 \times 50 \mu m^2$area and a thickness of $90nm$. The array holes are spaced more or less evenly apart in the x and y direction at . Due to the varying E-beam parameters the hole size differs between $160 \times 160 nm^2$ and $592 \times 592 nm^2$.

(a) SEM imaging overview of arrays

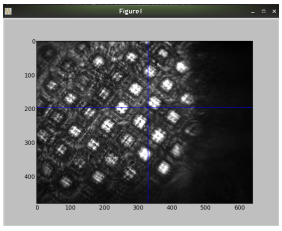


(b) Sample viewed through current experimental setup

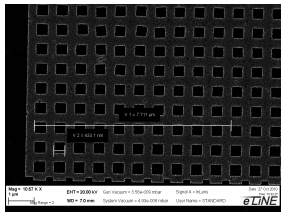

(c) SEM imaging overview of single array

Figure 3.4: Sample images

## 3.5 Methodology

The sample is viewed in reflection with a camera (Prosilica, EC 650) at $900nm$, which gives the best contrast to find the desired array. A lens with a $150mm$ focal length is placed on the optical rails before the focusing component and the beam splitter that deflects the reflection towards the camera. That way the beam spot is blown up and we can do wide field illumination on the sample. Focussing is done by moving the vertical component with a micrometre screw until the sample is in focus with the $150mm$ lens in place. When the sample is in focus this $150mm$ lens is removed and as a result the laser beam is then focused to aspect of a $30\mu m$ diameter. The AOTF then scans through the driving frequency effectively scanning through the wavelength spectrum. During the scan the transmitted beam is collimated and focused on a photodiode which is connected to a National Instruments card that collects the data onto the PC.

We find that the intensity of wavelengths at the borders of our spectrum is very low and for a sweep over the entire spectrum insufficient resolution is acquired. Therefore the measurement is divided in three sweeps from $480nm$ to $660nm$, $660nm$ to $840nm$ and $840nm$ to $1020nm$. The laser is kept constantly at 100% intensity. The power output of the AOTF is chosen at maximum without the photodiode clipping the signal.

Each active single measurement constitutes of 10 individual automated measurements conducted within seconds. The 10 data sets are then averaged to give the final data.

# 4 Results

In this chapter the outcome of our measurements are presented. An overview is given of the transmission spectroscopy on the various hole arrays. The relative transmission is then used to compare the individual arrays and to weigh those results against established spectroscopy techniques.

## 4.1 Transmission Spectroscopy using an AOTF

### 4.1.1 Measured Transmission

Each of the 9 selected arrays (see (3.4)), denoted by $\alpha$ through $\rho$, is singularly illuminated by the laser while the wavelengths of its spectrum are scanned through and the following transmission is collected by the photodiode, using the setup and method from section (3).

The axes of the individual graphs in figure (4.1) show the wavelengths calibrated against the time of the sweep and the measured voltage by the photodiode at that time. The graphs clearly constitutes out of three regions (blue, red and green) as the scan through the entire spectrum was divided in three separate scans according to section (3.5). For each region the figures all contain two graphs; the dashed line is the measured transmission through the corresponding array and the solid line depicts the reference measurement done through the glass, described in (3.5). Figure (4.1) shows that for all the arrays we find a somewhat linear relation between the relative transmission and the incident wavelength.

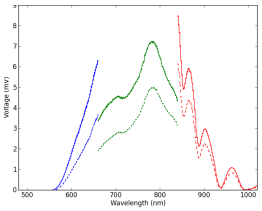


(a) Array $\alpha$ has different sized apertures irregularly spread out across the array

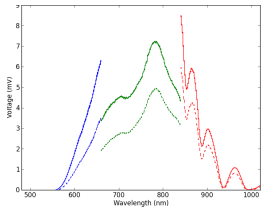


(b) Array $\beta$ has a aperture diameter: $211.3nm$ and a hole-to-hole pitch of $767.9nm$

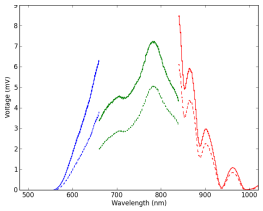


(c) Array $\gamma$ has a aperture diameter: $253.5nm$ and a hole-to-hole pitch of $773.2nm$

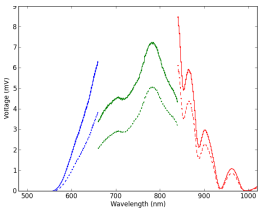


(d) Array $\delta$ has a aperture diameter: $338.0nm$ and a hole-to-hole pitch of $769.0nm$

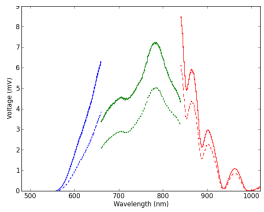


(e) Array $\varepsilon$ has a aperture diameter: $401.4nm$ and a hole-to-hole pitch of $770.0nm$

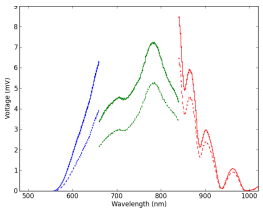


(f) Array $\kappa$ has a aperture diameter: $570.4nm$ and a hole-to-hole pitch of $771.1nm$

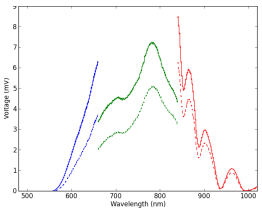


(g) Array $\lambda$ has a aperture diameter: $485.9nm$ and a hole-to-hole pitch of $771.1nm$

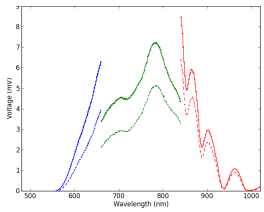


(h) Array $\mu$ has a aperture diameter: $433.1nm$ and a hole-to-hole pitch of $771.1nm$

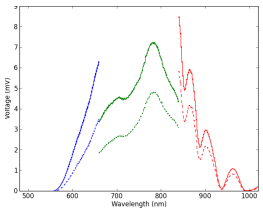


(i) Array $\rho$ has a aperture diameter: $306.3nm$ and a hole-to-hole pitch of $765.8nm$

Figure 4.1: Directly measured transmission trough the thin gold film arrays plotted in the same figure as the transmission measured through the glass

The incident intensity of the different wavelengths clearly varies strongly and accordingly we find roughly the same shape in the transmission graph through the gold arrays as through the glass. The intensity distribution across the spectrum is due to the laser (section (3.2.2)) which also shows increasing peaks in intensity at around $870nm$, $900nm$ and $970nm$. Normalization will compensate for this.

### 4.1.2 Normalized Transmission

For an array-to-array comparison the measured transmission is normalized by dividing it by the transmission measured through the glass so we get the relative transmission. Due to the normalization steep peaks occur at the borders of the spectrum where the intensity is to low and the fraction approaches infinity of zero. These peaks do not represent actual physics phenomena and are solely due to the data processing. Discarding those regions, the relative transmission results in a nice nearly linear plot for the $600 - 900nm$ range. Outside of those borders the intensity still was too low to measure reliable transmittance.

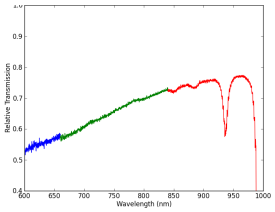


(a) Array $\alpha$ has different sized apertures irregularly spread out across the array

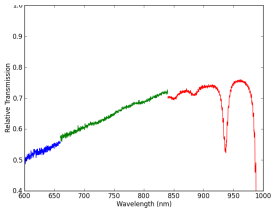


(b) Array $\beta$ has a aperture diameter: $211.3nm$ and a hole-to-hole pitch of $767.9nm$

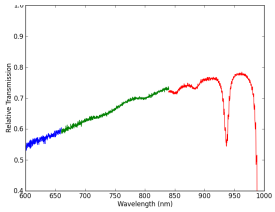


(c) Array $\gamma$ has a aperture diameter: $253.5nm$ and a hole-to-hole pitch of $773.2nm$

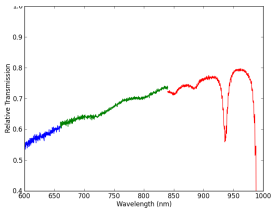


(d) Array $\delta$ has a aperture diameter: $338.0nm$ and a hole-to-hole pitch of $769.0nm$

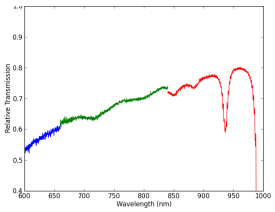


(e) Array $\varepsilon$ has a aperture diameter: $401.4nm$ and a hole-to-hole pitch of $770.0nm$

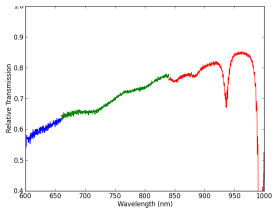


(f) Array $\kappa$ has a aperture diameter: $570.4nm$ and a hole-to-hole pitch of $771.1nm$

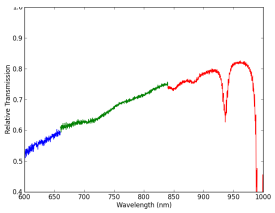


(g) Array $\lambda$ has a aperture diameter: $485.9nm$ and a hole-to-hole pitch of $771.1nm$

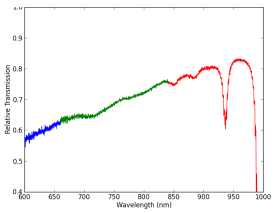


(h) Array $\mu$ has a aperture diameter: $433.1nm$ and a hole-to-hole pitch of $771.1nm$

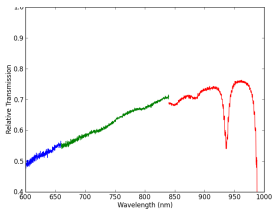


(i) Array $\rho$ has a aperture diameter: $306.3nm$ and a hole-to-hole pitch of $765.8nm$

Figure 4.2: Relative Transmission calculated by dividing the transmission through the sample by the transmission through glass in the well defined regime $600 - 1000nm$, see the appendices A for the entire graph

On the right side of each graph still two (negative) peaks due to the normalization mentioned above. Figure (4.2) shows that the relative transmission for the arrays $\alpha$ through $\rho$ lies between 0.5 and 0.8 meaning that at the least half of the incident light is transmitted. Furthermore we clearly recognize a linear-like increase of the transmission for increasing wavelength. Finally we report anomalies in the relative transmission consistently occurring for all the arrays at, by approximation, the same wavelengths. Most prominent of these are the decreases in the red part of the transmission graph for all arrays at around $850nm$ and $890nm$. Also for the arrays $\gamma$ through $\mu$ we see a less strong decrease in relative transmission in the green part of the graph for the $720nm - 730nm$ regime as can be seen in figures (4.2c) through (4.2h).

## 4.2 Comparison to Transmission Spectroscopy by Broadband Illuminating

In 2012 spectroscopy analysis was done on these same samples by *R. Pos et al.[10]* using a different, more common method. A comparison with the results found by *R. Pos et al.* will evaluate this technique by means of an AOTF. Figure (4.3) shows the relative transmissions measured by *R. Pos et al.*

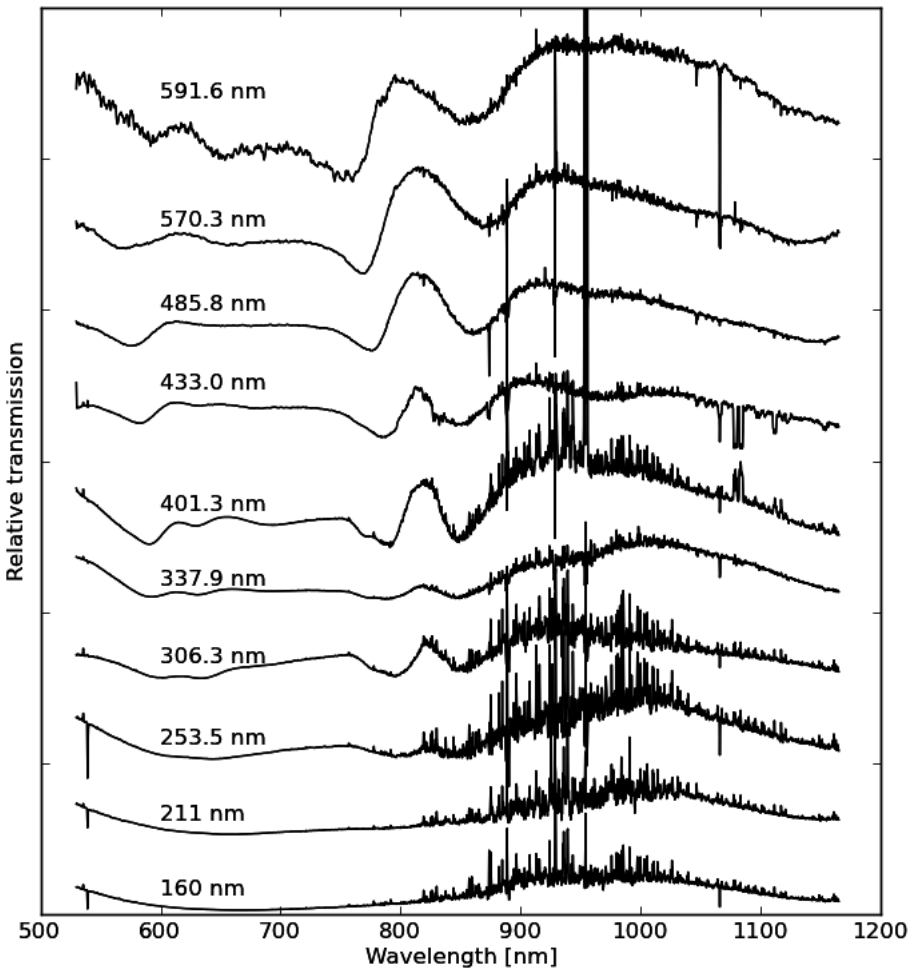


Figure 4.3: Relative Transmission graph from *R. Pos et al.*[10] from bottom to top the graphs correspond to the following arrays: $\alpha, \beta, \gamma, \rho, \delta, \epsilon, \mu, \lambda, \kappa$ and the top graph does not correspond to any of the measured arrays
**Original caption:** Measured eot spectrum for a periodic structure on a gold film. The pitch of the structure was 770 nm, while holesizes varied from 160nm to 592 nm, in steps of roughly 50 nm. The relative transmission is the measured transmitted intensity through the structure divided by the intensity as measured in the absence of the structure (e.g. through plain glass). Graphs have been vertically shifted for clarity.

Figure (4.3) shows some striking differences with the measured transmission in section (4.1.2). The transmission, as measured by *R. Pos et al* does not show the same linear increase for all the arrays, nor any decrease in transmission in the$720nm - 730nm$ regime for any arrays whatsoever. It does show however two decreasing anomalies as measured in this study, although less clear and shifted slightly at shorter wavelengths of around $800nm$ and $850nm$. More importantly

the more sharpy visible increase between these decreases is absent in this study's measurements.

Another distinctive difference is the large amount of noise in the transmission graphs of figure (4.3), making it hard to determine the actual transmission. The measurements done for this research are free of this drawback because of the increased intensity during the scan through that wavelength region.

A quantitative comparison of the relative transmissions is obviously impossible due to the use of arbitrary units so the high relative transmission measured in section (4.1.2) can not be checked.

Finally the results from the AOTF-spectroscopy show far less variation for all the arrays in transmission per wavelength over the entire spectrum.

# 5 Conclusion

The goal of this research was to evaluate a novel method for spectroscopy purposes using acousto-optic tuneable filters. Using these AOTF's the transmission through sub-wavelength hole arrays in a thin gold film was measured. At high speed the AOTF's scanned through the entire range of acoustic frequencies, effectively filtering out many narrowband spectra by diffracting a very narrowband optical spectrum at a time. Consequently the transmission of each singular narrowband light spectrum was also measured at a time resulting into the total transmission spectrum plotted against time.

This technique enables amplification of the intensity of otherwise weakly present wavelengths in respect to the total spectrum. This ensures enough intensity for all the wavelengths for spectroscopy measurements within the studied spectrum, the benefit of which is a great reduction of relative noise for the weak intensity wavelengths. This results in a much more accurate graph of the measurement over a much broader spectrum.

Comparison of the relative transmission with earlier research conducted on the same sample but with another method of spectroscopy showed deviating results. The anomalies due to extraordinary optical transmission or diffraction in the transmission spectrum expected from theory or found in earlier research, were absent in this study's measurements. The reason for the absence of these anomalies remains unclear.

A conclusive answer regarding the advantage of an AOTF for spectroscopy goals is not yet possible on solely this study. It has shown to offer some advantages in comparison to other methods but still further research is required.

# 6 Outlook

The use of acousto-optic tuneable filters for spectroscopy purposes shows promising prospects, however the transmission results differ strongly from earlier findings an theoretical predictions. A number of possibilities as to why this is the case exist and should be investigated in the future.

First of all should be taken into account that the theory addressed for this study to describe transmission is applicable for incident plane waves, that is incident waves with identical k-vectors and without phase difference. The current setup uses a focused beam so the k-vector vary in the x, y and z direction. Therefore you get an unknown averaging over all the different k-vectors present in the beam and would it be beneficial to also explore the outcome for a incident plane wave.

Secondly it has been a disadvantage that the monitoring of the sample was done in reflection while we were interested in the transmission spectroscopy. Due to time constraint was it not possible to change this but future measurements conducted this way would probably be an improvement.

Thirdly due to the divergence in the laser beam and the very small scale of the arrays it was necessary to focus the beam and the only manner to find the sample was to use the $150mm$ lens to do wide field illumination, focus on the array and do the measurements without being able to know for certain that the laser spot still was within the array. It would explain the high measured transmission and lack of structure in the transmission graph. Without the focussing and by implementing a pinhole it should be possible to avoid this problem in the future.

Finally different wavelengths were used in the measurement, while finding the sample and focussing onto it using a single narrowband spectrum. Not being able to see the sample during measurements could have made it well possible that the spot location varied for different wavelengths due to chromatic aberrations in the setup, which prior to this study has only been used for a single wavelength. Again the pinhole or simply larger arrays could avoid this risk that the spot could get off target.

# 7 Acknowledgments

The last five months, in which this research was conducted, I had the pleasure working with a group of very friendly and helpful people, without whom this study would not be in front of you today. I would like to express my appreciation for their constant support and advise throughout.

First of all, I would like to my supervisor dr. Dries van Oosten for his guidance during this research. His enthusiasm on the subject inspired and his willingness to share his knowledge was essential in keeping the focus on the relevant physics for this study.

Secondly my thanks go out to prof. dr. Jaap Dijkhuis as head of the department and prof. dr. Denise Krol, for their constant presence during our meetings and for always being prepared to think along and discuss our findings.

Next, I am very thankful to ing. Cees de Kok, who I could always trouble for his knowledge on all the technical components used in the setup. His advice was paramount for the setup development described in this paper.

Of course I would also very much thank Hao Zhang and Ole Mussman for respectively the use of his old experimental setup and for the providing of the samples. These obviously were key aspects for this research and their willingness to provide en elaborate on them is very much appreciated.

Nearly not a single day during the research went by without the excellent support and advice of Stephan Wolbers and Bruno van Albada. Their day-to-day guidance was very important in the completion of this study, specifically by showing me around Python and all the experimental techniques needed for the research.

Finally I would like to thank the Debye Institute for the interesting and pleasant experience of carrying out my bachelor research there.

# References

[1] H. Bethe. Theory of diffraction by small holes. *Physical Review*, 66(7-8):163–182, 1944.

[2] T. Y. Choi and C. P. Grigoropoulos. Plasma and ablation dynamics in ultrafast laser processing of crystalline silicon. *Journal of applied physics*, 92(9):4918–4925, 2002.

[3] B. H. Christensen, K. Vestentoft, and P. Balling. Short-pulse ablation rates and the two-temperature model. *Applied surface science*, 253(15):6347–6352, 2007.

[4] T. W. Ebbesen, H. Lezec, H. Ghaemi, T. Thio, and P. Wolff. Extraordinary optical transmission through sub-wavelength hole arrays. *Nature*, 391(6668):667–669, 1998.

[5] Z. Fan, L. Zhan, X. Hu, and Y. Xia. Critical process of extraordinary optical transmission through periodic subwavelength hole array: Hole-assisted evanescent-field coupling. *Optics Communications*, 281:5467–5471, Nov. 2008.

[6] J. R. Hook and H. E. Hall. *Solid State Physics (The Manchester Physics Series)*. John Wiley and Sons Ltd, 2000.

[7] J. Jacobs. A set-up to measure the infuence of split ring resonators on spontaneous emission. Master's thesis, Utrecht University, 2009.

[8] J. Kaakkunen, K. Paivasaari, and P. Vahimaa. Fabrication of large-area hole arrays using high-efficiency two-grating interference system and femtosecond laser ablation. *Applied Physics A*, 103(2):267–270, 2011.

[9] H. Liu and P. Lalanne. Microscopic theory of the extraordinary optical transmission. *Nature*, 452(7188):728–731, 2008.

[10] R. Pos. Extraordinary optical transmission through periodic structures in gold. Master's thesis, Utrecht University, 2012.

[11] F. W. Sears, M. W. Zemansky, and H. D. Young. *University physics*, volume 1. Addison-Wesley Reading, UK, 2006.

[12] F. van Beijnum, C. Rétif, C. Smiet, and M. van Exter. Transmission processes in random patterns of subwavelength holes. *Opt. Lett.*, 36(18):3666–3668, Sept. 14th 2011.

[13] F. van Beijnum, C. Rétif, C. B. Smiet, H. Liu, P. Lalanne, and M. P. van Exter. Quasi-cylindrical wave contribution in experiments on extraordinary optical transmission. *Nature*, 492:411, Dec. 20th 2012.

[14] A. S. Vengurlekar. Extraordinary optical transmission through metal films with sub wavelength holes and slits. *arXiv preprint arXiv:1004.0603*, 2010.

[15] H. Zhang, D. van Oosten, D. M. Krol, and J. I. Dijkhuis. Saturation effects in femtosecond laser ablation of silicon-on-insulator. *Applied Physics Letters*, 99(23):231108, Dec. 2011.

# A Appendices

## Uncut Relative Transmission

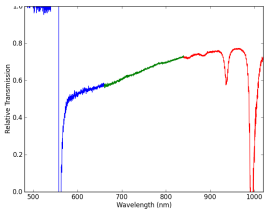


(a) Array $\alpha$ has different sized apertures irregularly spread out across the array

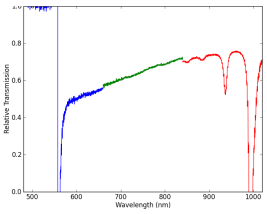


(b) Array $\beta$ has a aperture diameter: $211.3nm$ and a hole-to-hole pitch of $767.9nm$

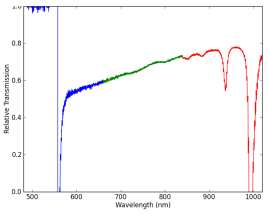


(c) Array $\gamma$ has a aperture diameter: $253.5nm$ and a hole-to-hole pitch of $773.2nm$

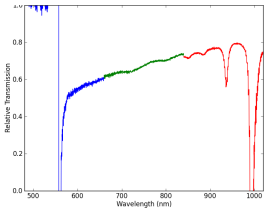


(d) Array $\delta$ has a aperture diameter: $338.0nm$ and a hole-to-hole pitch of $769.0nm$

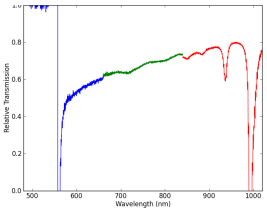


(e) Array $\varepsilon$ has a aperture diameter: $401.4nm$ and a hole-to-hole pitch of $770.0nm$

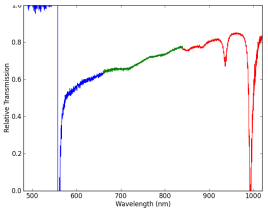


(f) Array $\kappa$ has a aperture diameter: $570.4nm$ and a hole-to-hole pitch of $771.1nm$

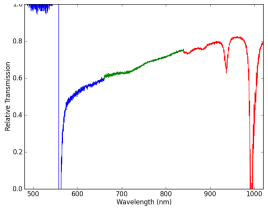


(g) Array $\lambda$ has a aperture diameter: $485.9nm$ and a hole-to-hole pitch of $771.1nm$

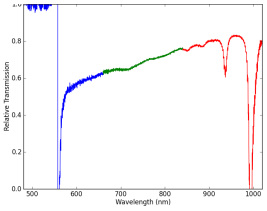


(h) Array $\mu$ has a aperture diameter: $433.1nm$ and a hole-to-hole pitch of $771.1nm$

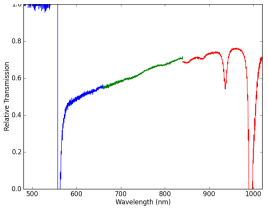


(i) Array $\rho$ has a aperture diameter: $306.3nm$ and a hole-to-hole pitch of $765.8nm$

Figure A.1: Uncut Relative Transmission

## Setup Model

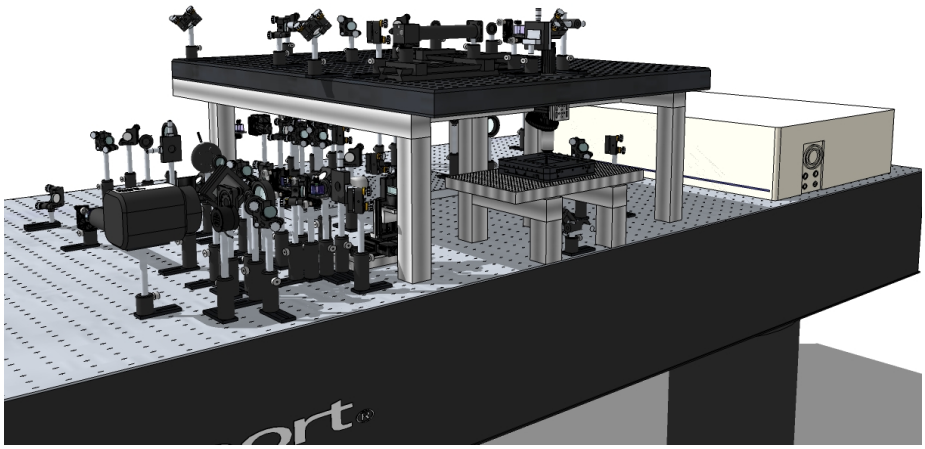

## Technical overview

| Apparatus | Brand | Model |
|---|---|---|
| Laser | NKT Photonics | SuperK Extreme EXR-4 |
| AOTF | Gooch & Housego | PCAOMNIR 1 |
| Camera | Prosilica | EC 650 |
| Sample mount | Physik Intrumente | M-686 XY |
| Spectrometer | Ocean Optics | HR2000CG-UV-NIR |
| Beamprofiling Camera | DataRay Inc | WinCamD-USDxx |
| Data Acquisition | National | CB-68LPR |

## Piëzo-stage Python control-script

```
#!/usr/bin/env python

import serial
import time, datetime
import os
import numpy as np

# ======================== INITIALIZATION ========================
# setting intial values
startx = 5.0
starty = 5.0
endx = 15.0
endy = 15.0
step = 1.0
vel = 100.0

# configuring the serial connections
ser_stage = serial.Serial(4, 115200, timeout=None, parity='N', stopbits=1)
ser_stage.isOpen()

main_directory = 'C:/Users/Adriaan/Pythonsaves/'
date = datetime.datetime.now()
datename = str(date.year) +'-'+ str(date.month).zfill(2) +'-'+ str(date.day).zfill(2


def init():
    # initializing the stage: finding the middle, setting velocities, servo-control=
    ser_stage.write(
        'SVO 1 1\n'
        'SVO 2 1\n'
        'VEL 1 100\n'
        'VEL 2 100\n'
        'FRF 1\n'
        'FRF 2\n')
    time.sleep(2)
    ser_stage.write('GOH\n')

    # creating map name
    main_directory = 'C:/Users/Adriaan/Pythonsaves/'
    date = datetime.datetime.now()
    datename = str(date.year) +'-'+ str(date.month).zfill(2) +'-'+ str(date.day).zfi
    directorylist=os.listdir(main_directory)
    j = 1
    k =  True

    if True:
        if len(directorylist) > 0:
            while(k):
                for i in range(len(directorylist)):
                    if (datename + '_' + str(j).zfill(2)) in directorylist[i]:
                        j = j + 1
                        break
                    elif i == len(directorylist)-1:
                        k = False

        new_folder = datename
        if not os.path.exists(main_directory + new_folder):
            os.makedirs(main_directory + new_folder)

    # returning initial settings
```

```
    print datename+' '+ str(date.hour).zfill(2)+':'+ str(date.minute).zfill(2)+':'+
    print "Using serial port: " +ser_stage.portstr
    ser_stage.write('POS?\n')
    print "Position x-axes: " +ser_stage.readline(), "Position y-axes: " +ser_stage.

# ======================== FUNCTIONS ========================

# Getting current position
def pos():
    ser_stage.write('POS?\n')
    time.sleep(0.02)
    print "Position:\r" +ser_stage.read(ser_stage.inWaiting())

# scalable function making a array, returning position and time measurement
def scale(nx,ny,dx,dy,hz):
    delay = 0.5 / hz
    print "Points on x-axes: " +str(nx)
    print "Points on y-axes: " +str(ny)
    print "Periodicity x-axes: " +str(dx)
    print "Periodicity y-axes: " +str(dx)
    print "Delay: " +str(delay)
    print "Estimated Run time: " +str((nx*ny)*(delay+0.2)) +'\n'

    ser_stage.write('MOV 1 ' + str(startx) + '\n')
    ser_stage.write('MOV 2 ' + str(starty) + '\n')
    time.sleep(1)

    ser_stage.write('POS?\n')
    time.sleep(0.2)
    t0 = time.clock()
    data = np.array([[t0, float(ser_stage.readline()[2:]), float(ser_stage.readline(
    j = 0
    while (j < ny):
        for i in range(1,nx):
            ser_stage.write('MVR 1 ' + str(dx) + '\n')
            time.sleep(delay)
            t = time.clock()
            ser_stage.write('POS?\n')
            time.sleep(0.2)
            output = [t, float(ser_stage.readline()[2:]), float(ser_stage.readline()
            data = np.append(data,[output],axis=0)
        j = j + 1

        if(j < ny):
            ser_stage.write('MVR 2 ' + str(dx) + '\n')
            time.sleep(delay)
            t = time.clock()
            ser_stage.write('POS?\n')
            time.sleep(0.2)
            output = [t, float(ser_stage.readline()[2:]), float(ser_stage.readline()
            data = np.append(data,[output],axis=0)
            for i in range(1,nx):
                ser_stage.write('MVR 1 -' + str(dx) + '\n')
                time.sleep(delay)
                t = time.clock()
                ser_stage.write('POS?\n')
                time.sleep(0.2)
                output = [t, float(ser_stage.readline()[2:]), float(ser_stage.readli
                data = np.append(data,[output],axis=0)
            j = j + 1
```

```
            if(j < ny):
                ser_stage.write('MVR 2 ' + str(dx) + '\n')
                time.sleep(delay)
                t = time.clock()
                ser_stage.write('POS?\n')
                time.sleep(0.2)
                output = [t, float(ser_stage.readline()[2:]), float(ser_stage.readli
                data = np.append(data,[output],axis=0)

    print data
    print "Total Process Time:", time.clock() - t0
    time.sleep(1)
    filename = main_directory + datename + "/" + "hole_array_"+str(date.hour).zfill(
    np.savetxt(filename, data, delimiter = ';')
    ser_stage.write('VEL 1 100\n')
    ser_stage.write('VEL 2 100\n')

    time.sleep(1)

    start()

# main function making a snake-like path
def main():
    stepsx = int((endx - startx) / step)
    stepsy = int((endy - starty) / step)
    delay = step/vel
    print stepsx
    print stepsy
    print delay

    ser_stage.write('MOV 1 ' + str(startx) + '\n')
    ser_stage.write('MOV 2 ' + str(starty) + '\n')
    time.sleep(1)
    ser_stage.write('VEL 1 ' + str(vel) + '\n')
    ser_stage.write('VEL 2 ' + str(vel) + '\n')

    t0 = time.clock()
    t1 = time.time()
    j = 0
    while (j < stepsy):
        for i in range(0,stepsx):
            ser_stage.write('MVR 1 ' + str(step) + '\n')
            time.sleep(delay)
        ser_stage.write('MVR 2 ' + str(step) + '\n')
        j = j + 1

        if(j < stepsy):
            for i in range(0,stepsx):
                ser_stage.write('MVR 1 -' + str(step) + '\n')
                time.sleep(delay)
            ser_stage.write('MVR 2 ' + str(step) + '\n')
            j = j + 1

    print t0, "t0"
    print time.clock(), "current time"
    print time.clock() - t0, "seconds process time"

    print t1, "t1"
    print time.time(), "current time"
```

```
    print time.time() - t1, "seconds wall time"


    time.sleep(1)
    ser_stage.write('VEL 1 100\n')
    ser_stage.write('VEL 2 100\n')

    time.sleep(1)

    start()

def start():
    ser_stage.write('MOV 1 ' + str(startx) + '\n')
    ser_stage.write('MOV 2 ' + str(starty) + '\n')

def fout():
    ser_stage.write('ERR?\n')
    out = ''
    # a small delay for device to respond
    time.sleep(0.01)
    while ser_stage.inWaiting() > 0:
        out += ser_stage.read(ser_stage.inWaiting())

    if(out != "") and (out != '0\n'):
        print "Unknown device command [Error: " + out + ']'

    else:
        print "No error occured"

def enter():
    print 'Enter your commands below.\r\nInsert "exit" to leave the application.'

    ser_stage.write('VEL 1 100.0\n')
    ser_stage.write('VEL 2 100.0\n')

    input=1
    while 1 :
        # get keyboard input
        input = raw_input(">> ")
            # Python 3 users
            # input = input(">> ")
        if input == 'exit':
            ser_stage.close()
            exit()
        elif input == '':
            print 'Python function not found'
        elif input[0] == '@':
            try:
                eval(input[1:])
            except:
                print 'Python function not found'
        else:
            # send the character to the device
            # N.B. a line feed (\n) is added - this is requested by my device

            ser_stage.write(input + '\n')
            out=''
            # a small delay for device to respond
            time.sleep(.05)
```

```
            while ser_stage.inWaiting() > 0:
                out+=ser_stage.read(ser_stage.inWaiting())

            if(out != ""):
                print "Output:\r" + str(out)

            # check if device has an error
            fout()

def timestep(x): # measure process time
    t0 = time.clock()
    time.sleep(x)
    print t0, "t0"
    print time.clock(), "current time"
    print time.clock() - t0, "seconds process time"

def getpos(n,x): # get positions of n steps
    ser_stage.write('VEL 1 100.0\n')
    ser_stage.write('VEL 2 100.0\n')
    ser_stage.write('POS?\n')
    time.sleep(0.2)
    data = np.array([[float(ser_stage.readline()[2:]), float(ser_stage.readline()[2:
    j = 1
    while (j < n+1):
        ser_stage.write('MVR 1 ' + str(x) + '\n')
        time.sleep(0.2)
        ser_stage.write('POS?\n')
        time.sleep(0.2)
        output = [float(ser_stage.readline()[2:]), float(ser_stage.readline()[2:])]
        data = np.append(data,[output],axis=0)
        j = j + 1

    time.sleep(0.5)
    ser_stage.write('GOH\n')
    print data

def timesteps(n,x): # time multiple steps
    ser_stage.write('VEL 1 100.0\n')
    ser_stage.write('VEL 2 100.0\n')
    j = 1
    print time.clock(), "starttijd"
    while (j < n+1):
        t = time.clock()
        print t, "tijd stap", str(j)
        ser_stage.write('MVR 1 ' + str(x) + '\n')
        print time.clock() - t, "tijdsduur stap", str(j)
        j = j + 1
    print time.clock(), "eindtijd"

    time.sleep(0.5)
    ser_stage.write('GOH\n')

def getpostime(n,x): # get positions and time measure of n steps
    ser_stage.write('VEL 1 100.0\n')
    ser_stage.write('VEL 2 100.0\n')
    ser_stage.write('POS?\n')
    time.sleep(0.2)
    j = 1
    t0 = time.clock()
    data = np.array([[t0, float(ser_stage.readline()[2:]), float(ser_stage.readline(
```

```
    while (j < n+1):
        ser_stage.write('MVR 1 ' + str(x) + '\n')
        time.sleep(0.2)
        t = time.clock()
        ser_stage.write('POS?\n')
        time.sleep(0.2)
        output = [t, float(ser_stage.readline()[2:]), float(ser_stage.readline()[2:]
        data = np.append(data,[output],axis=0)
        j = j + 1

    print t0, "Start Time"
    print time.clock(), "Finish Time"
    time.sleep(0.5)
    ser_stage.write('GOH\n')
    print data

def help():
    ser_stage.write('HLP?\n')
    out1=''
    out2=''
    time.sleep(.5)
    out1+=ser_stage.read(ser_stage.inWaiting())
    out2+=ser_stage.read(ser_stage.inWaiting())
    print out1
    print out2

def macro():
    ser_stage.write('MAC?\n')
    out=''
    time.sleep(.1)
    while ser_stage.inWaiting()>0:
          out+=ser_stage.read(1)
    print out

# main function making a snake-like path with controller macro's
def defmac():
    ser_stage.write('MAC BEG HOME\n')
    ser_stage.write('WAC #8 1\n')
    ser_stage.write('GOH\n')
    ser_stage.write('MAC END\n')

def mac(nx,ny,dx,dy):
    print "Points on x-axes: " +str(nx)
    print "Points on y-axes: " +str(ny)
    print "Periodicity x-axes: " +str(dx)
    print "Periodicity y-axes: " +str(dx)
#    print "Estimated Run time: " +str((nx*ny)*(delay+0.2)) +'\n'

    ser_stage.write('MOV 1 ' + str(startx) + '\n')
    ser_stage.write('MOV 2 ' + str(starty) + '\n')
    ser_stage.write('VEL 1 ' + str(vel) + '\n')
    ser_stage.write('VEL 2 ' + str(vel) + '\n')

    ser_stage.write('MAC BEG heen\n')
    ser_stage.write('MVR 1 ' +str(dx)+'\n')
    ser_stage.write('DEL 100\n')
    ser_stage.write('MAC END\n')

    ser_stage.write('MAC BEG weer\n')
    ser_stage.write('MVR 1 -' +str(dx)+'\n')
```

```
    ser_stage.write('DEL 100\n')
    ser_stage.write('MAC END\n')

    ser_stage.write('MAC BEG raster\n')
    ser_stage.write('MVR 2 ' +str(dy)+'\n')
    ser_stage.write('DEL 100\n')
    ser_stage.write('MAC NSTART heen ' +str(nx)+ '\n')
    ser_stage.write('MVR 2 ' +str(dy)+'\n')
    ser_stage.write('DEL 100\n')
    ser_stage.write('MAC NSTART weer ' +str(nx)+ '\n')
    ser_stage.write('MAC END\n')

    print time.clock(), "starttime"
    ser_stage.write('MAC NSTART raster ' +str(ny)+ '\n')
    print time.clock(), "Finish Time"

    time.sleep(3)
#    ser_stage.write('MAC START HOME\n')

# ========================= SCRIPT RUN =========================
init()
enter()
```